Electrochimica Acta 182 (2015) 391–397

Contents lists available at ScienceDirect

Electrochimica Acta

journal homepage: www.elsevier.com/locate/electacta

Bamboo-like multiwalled carbon nanotubes dispersed in double stranded calf-thymus DNA as a new analytical platform for building layer-by-layer based biosensors

Emiliano N. Primo, Fabiana A. Gutierrez, María D. Rubianes*, Gustavo A. Rivas*

INFIQC Departamento de Fisicoquímica, Facultad de Ciencias Químicas, Universidad Nacional de Córdoba, Ciudad Universitaria, 5000 Córdoba, Argentina

ARTICLE INFO

Article history:
Received 13 July 2015
Received in revised form 3 September 2015
Accepted 5 September 2015
Available online 8 September 2015

Keywords:
Carbon nanotubes functionalization
calf-thymus double stranded DNA
Glucose Oxidase
Layer-by-layer
Self-assembly
Electrochemical glucose biosensor
Bamboo-like carbon nanotubes

ABSTRACT

This work reports the successful application of bamboo-like multiwalled carbon nanotubes (bCNT) non-covalently functionalized with calf-thymus double stranded DNA (dsDNA) as a robust platform (bCNT-dsDNA) to build electrochemical biosensors. The "model system" proposed here as a proof of concept was an enzymatic biosensor devoted to glucose quantification obtained by layer-by-layer self-assemby of polydiallyldimethylammonium (PDDA) and glucose oxidase (GOx) at glassy carbon electrodes (GCE) modified with bCNT-dsDNA (GCE/bCNT-dsDNA/$(PDDA/GOx)_n$). The influence of GOx and PDDA assembling conditions and the effect of the number of PDDA/GOx bilayers (n) on the performance of the resulting biosensor is critically discussed. The supramolecular architecture was characterized by electrochemical impedance spectroscopy from the charge transfer resistance of quinone/hydroquinone and potassium ferrocyanide/potassium ferricyanide; by cyclic voltammetry from the surface concentration of GOx using ferrocene methanol as enzyme regenerator; by amperometry from the response of the enzymatically generated hydrogen peroxide; and by surface plasmon resonance from the changes in the plasmon resonance angle. The analytical parameters obtained with GCE/bCNT-dsDNA/$(PDDA/GOx)_3$ for the amperometric quantification of glucose at 0.700 V were: sensitivity of (265 ± 7) $\mu A\,mM^{-1}\,cm^{-2}$, linear range between 0.25 and 2.50×10^{-3} M, detection limit of 50 μM, repeatability of 3.6% (n = 10), and negligible interference from maltose, galactose, fructose and manose. The biosensor was successfully used for the sensitive quantification of glucose in beverages and a medicine sample.

1. Introduction

The development of efficient biosensors is of great importance in different areas, ranging from clinical and environmental chemistry to biotechnological and industrial production [1]. In this sense, electrochemical biosensors have demonstrated exceptional attributes such as being sensitive, portable, simple-to-construct, easy-to-operate and economical [2]. Particularly, nanomaterials-based electrochemical biosensors have received great attention due to the advantages of functional nanomaterials mainly connected with tunability, versatility, self-assembling ability and possibility to amplify biorecognition events [3]. CNTs have been widely used for the development of electrochemical biosensors due to their exceptional properties, like large surface-to-volume ratio, high mechanical strength, faster electron transfer kinetics, excellent chemical and thermal stability, and high surface density for the immobilization of biomolecules [4,5].

Layer-by-layer (LbL) self-assembly of polymer and nanomaterials has demonstrated to be a very useful tool for the fabrication of nanostructured films with high organization at the nanoscale level due to the inherent simplicity, versatility and universality [6–11]. CNTs have been used for the development of electrochemical biosensors built by LbL following different strategies: by using the nanostructures as starting platform for further assembling of polyelectrolytes; as an active support to bring biorecognition molecules or polyelectrolytes; or as source of negative charges to allow further electrostatic interaction with polycations [12–14]. Dalmasso and coworkers [15] have proposed a glucose biosensor obtained by alternate deposition of GOx and CNT dispersed with polyhystidine (CNT-Polyhis) at glassy carbon electrodes (GCE). They reported the successful assembling of five (CNT-PHys/GOx) bilayers with the consequent increase in glucose sensitivity. In a similar way, Ma et al. [16] have developed a glucose biosensor by immobilizing eight (polydiallyldimethyl ammonium/GOx) bilayers at Au/thionine/CNT/$(polyacrylic\ acid/polyvinylstyrene)_3$, where

* Corresponding author. Tel.: +54-351-5353866; fax: +54-351-4334188.
E-mail addresses: rubianes@fcq.unc.edu.ar (M.D. Rubianes), grivas@fcq.unc.edu.ar (G.A. Rivas).

http://dx.doi.org/10.1016/j.electacta.2015.09.028
0013-4686/

CNTs were vertically aligned at the gold surface. In a different approach, Zhang and coworkers [17] have developed biosensors for discriminative detection of organophosphorus pesticides by assembling CNT dispersed with polyethyleneimine (PEI), DNA, acetylcholine esterase (AChE) and organophosphate hydrolase (OPH) at GCE. The authors have used CNT-PEI and CNT-DNA as "cushion layers" for further deposition of the biosensing elements supported by CNTs (CNT-AChE and CNT-OPH), reporting that the best compromise between sensitivity towards the analytes and conductivity/resistivity of the films was attained with GCE/(CNT-PEI/CNT-DNA)$_2$/CNT-AChE/CNT-OPH. However, even when, different strategies for the construction of CNT-LbL based biosensors have been reported [18–20], is important to remark that extensive study is still required to fully understand the factors that govern and improve the analytical signals [21].

We have recently reported the excellent electrochemical behavior of glassy carbon electrodes (GCE) modified with bamboo-like MWCNT dispersed in calf-thymus dsDNA [22]. The dsDNA that supports the bCNTs maintained its bioaffinity properties, even after the drastic conditions to prepare the dispersion (use of ethanol/water and sonication), making possible the successful recognition of the intercalator promethazine, its selective preconcentration and its quantification at nanomolar level [22,23].

The aim of this work is to demonstrate the usefulness of bCNT non-covalently functionalized with dsDNA (GCE/bCNT-dsDNA) as a platform to build electrochemical biosensors taking advantage of the unique properties of bCNT, the characteristic of negatively charged backbone of dsDNA, and the robustness of bCNT-dsDNA. We propose the GCE/bCNT-dsDNA platform as a "model biosensing system" using glucose oxidase (GOx) as biorecognition element immobilized by alternate LbL assembling of polydiallyldimethylamonium (PDDA) and glucose oxidase (GOx). The supramolecular multistructure was characterized using amperometry, cyclic voltammetry (CV), electrochemical impedance spectroscopy (EIS) and surface plasmon resonance (SPR). In the following sections we will discuss the influence of the PDDA and GOx adsorption conditions and the number of PDDA/GOx layers on the analytical performance of the resulting biosensing platform.

2. Experimental

2.1. Reagents

D-(+)-glucose (Glu), D-(+)-manose (Man) and D-(+)-galactose (Gal) were obtained from Merck. Maltose (Mal) and fructose (Fru) was purchased from Mallinckrodt. Glucose oxidase (GOx) (Type X-S, Aspergillus niger, EC 1.1.3.4, 158,900 units per gram of solid), calf-thymus double stranded DNA (dsDNA) (Catalog number D 4522), ferrocene methanol (FcOH), poly-diallyldimethylammonium chloride (PDDA) (MW=100,000–200,000), potassium ferrocyanide, and potassium ferricyanide were obtained from Sigma. Bamboo-like multiwalled carbon nanotubes (bCNT, diameter (30 ± 10) nm, length 1–5 μm, 98.92% purity) were obtained from NanoLab (U. S.A.). Other chemicals were analytical reagent grade and used without further purification.

PDDA and GOx solutions were prepared in ultrapure water and 0.050 M phosphate buffer solution pH 7.40, respectively. The stock solutions of Glu, Gal, Man, Mal, and Fru were prepared in 0.050 M phosphate buffer solution pH 7.40 before starting each set of experiments. All aqueous solutions were prepared with ultrapure water (ρ=18 MΩcm) from a Millipore-MilliQ system.

2.2. Apparatus

Amperometric measurements were performed with a TEQ_04 potentiostat while cyclic voltammetry and EIS experiments were carried out with an Autolab PGSTAT 128N potentiostat (EcoChemie). SPR measurements were done with a single channel Autolab SPRINGLE instrument (Eco Chemie).

Glassy carbon electrodes (GCE, CH Instruments, 3 mm diameter) were used as working electrodes. A platinum wire and Ag/AgCl, 3 M NaCl served as counter and reference electrodes, respectively. All potentials are referred to the latter. The electrodes were inserted into the electrochemical cell through holes in its Teflon cover. A magnetic stirrer provided the convective transport during the amperometric measurements.

2.3. Preparation of the working electrode

2.3.1. Preparation of GCE modified with bCNT-dsDNA (GCE/bCNT-dsDNA)

The dispersion of bCNTs with dsDNA was prepared following the protocol previously reported [22]. Briefly, 1.00 mL of 100 ppm dsDNA solution (prepared in 50% v/v ethanol:water) was added to 1.00 mg of bCNT powder, sonicated for 45 min, and centrifuged at 9000 rpm for 15 min.

Before modification, the GCEs were polished with alumina slurries of 0.3 and 0.05 μm for 1.0 min each and then sonicated in water for 10 s. After that, 20 μL of the bCNT-dsDNA dispersion was casted over the GCE followed by the evaporation of the solvent by exposure to air for 90 min.

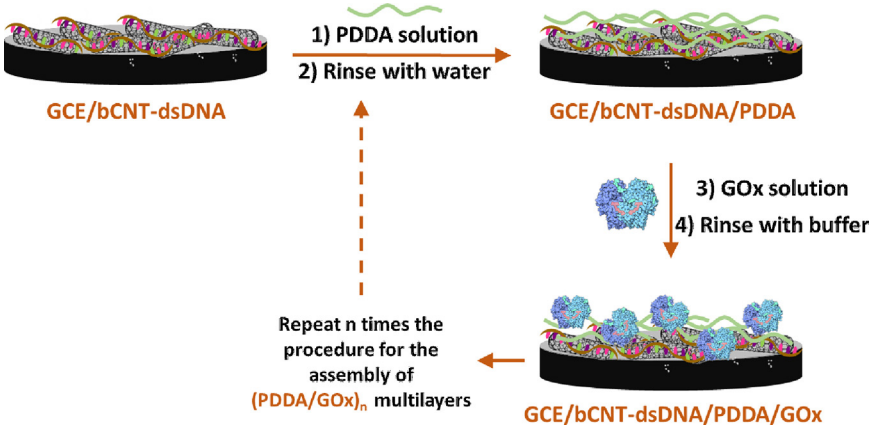

Fig. 1. Scheme of the LbL self-assembly of PDDA and GOx at GCE/bCNT-dsDNA.

2.3.2. Construction of PDDA/GOx multilayers films at GCE/bCNT-dsDNA (GCE/bCNT-dsDNA/PDDA/GOx)$_n$

The biosensor was obtained by immersion of GCE/bCNT-dsDNA in a 0.50 mg mL^{-1} PDDA solution for 5.0 min followed by immersion in a 1.00 mg mL^{-1} GOx solution for 15.0 min, as illustrated in Fig. 1. The multilayered system was obtained by repeating the previous scheme and the resulting electrodes were named GCE/bCNT-dsDNA/(PDDA/GOx)$_n$, being *n* the "number of bilayers" or more strictly, the number of PDDA/GOx adsorption steps. After each adsorption step, the surfaces were copiously rinsed with the medium used for preparing the polyelectrolyte solution.

2.4. Procedure

Amperometric experiments were carried out by applying 0.700 V and allowing the transient current to decay to a steady-state value prior to the addition of the analyte and the subsequent current monitoring. EIS experiments were performed by applying a sinusoidal potential perturbation of 10 mV amplitude in the frequency range between 10^5 and 10^{-1} Hz and a working potential corresponding to the formal potential of 2.0×10^{-3} M $[Fe(CN)_6]^{3-/4-}$ (0.210 V) or 2.0×10^{-3} M H_2Q/Q (~0.050 V). The impedance spectra were analyzed by using the Z-view program.

For SPR measurements, the Au SPR sensor disks (BK 7) were modified *ex-situ* by deposition of 20 μL of 0.30 mg mL^{-1} bCNT-dsDNA dispersion and further drying at room temperature. The SPR disks were mounted on a hemicylindrical lens through index-matching oil to form the base of the cuvette. The measurements were carried out under non-flow liquid conditions at 25 °C.

The results presented here were obtained using three different dispersions and three electrodes in each case. All the experiments were conducted at room temperature.

3. Results and discussion

The rational design of LbL-based biosensors requires a critical analysis of the concentration and deposition time of the polyelectrolytes and the number of biorecognition layers that the architecture can support. In the following sections we will discuss the influence of these parameters on the analytical performance of the resulting GCE/bCNT-dsDNA/(PDDA/GOx)$_n$ supramolecular multistructure. We will use the sensitivity to glucose obtained from amperometric experiments at 0.700 V as the main analytical parameter for selecting the experimental conditions. Fig. 2 shows a typical amperogram obtained at GCE/bCNT-dsDNA/(PDDA/GOx)$_n$ for successive additions of glucose. The inset depicts the corresponding calibration plot.

3.1. Effect of PDDA and GOx concentration and adsorption time

The effect of PDDA concentration and adsorption time on the performance of the resulting biosensors was studied from amperometric experiments performed at 0.700 V after successive additions of 5.0×10^{-4} M glucose (Fig. S1). The electrodes were prepared using different PDDA concentrations (from 0.50 to 2.00 mg mL^{-1}) and different deposition times (from 5.0 to 15.0 min) followed by the self-assembling of 1.00 mg mL^{-1} GOx for 15.0 min. The sensitivity is rather independent of PDDA adsorption time, and the concentration of PDDA demonstrated to have just a small influence on the sensitivity to glucose. For instance, by increasing the PDDA concentration from 0.50 to 1.00 mg mL^{-1}, the sensitivity only rises 26%. Therefore, the selected conditions for PDDA adsorption were 0.50 mg mL^{-1} and 5.0 min deposition.

The conditions for GOx self-assembly at GCE/bCNT-dsDNA/PDDA were also evaluated from amperometric experiments performed at 0.700 V for successive additions of 5.0×10^{-4} M glucose. The biosensors were prepared using different GOx deposition times (from 5.0 to 15.0 min) and several concentrations (from 0.25 to 2.00 mg mL^{-1}). Fig. 3 illustrates the effect of these parameters on the sensitivity of the resulting biosensors. The sensitivity increases with the concentration of GOx either for 5.0, 10.0 or 15.0 min adsorption. The best compromise between sensitivity, stability, reproducibility, and linear range was achieved with the platform obtained by adsorption of 1.00 mg mL^{-1} GOx for 15.0 min. Therefore, these conditions were selected for further work.

3.2. Effect of the number of (PDDA/GOx) bilayers

Fig. 4 displays the effect of the number of PDDA/GOx bilayers at GCE/bCNT-dsDNA/(PDDA/GOx)$_n$ on the sensitivity to glucose obtained from amperometric experiments at 0.700 V. The

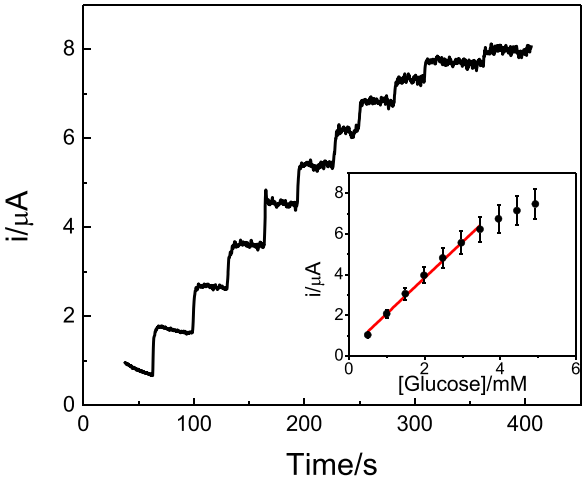

Fig. 2. Amperometric recording obtained at GCE/bCNT-dsDNA/PDDA/GOx after successive additions of 5.0×10^{-4} M glucose. Working potential: 0.700 V. Supporting electrolyte: 0.050 M phosphate buffer solution pH 7.40. Inset: calibration plot obtained from the amperometry. The red line shows the linear fit to the data.

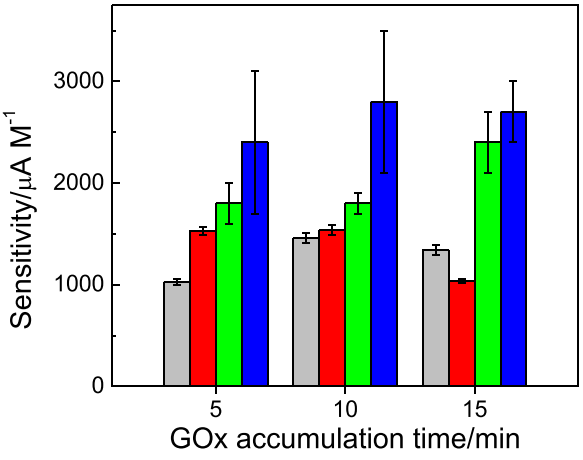

Fig. 3. Glucose sensitivity of GCE/bCNT-dsDNA/PDDA/GOx as a function of GOx accumulation time. Gray bars corresponds to GOx 0.25 mg mL^{-1}; red bars, to GOx 0.50 mg mL^{-1}; green bars, to GOx 1.00 mg mL^{-1}; and blue bars, to GOx 2.00 mg mL^{-1}. Working potential: 0.700 V. Supporting electrolyte: 0.050 M phosphate buffer solution pH 7.40. PDDA adsorption conditions: 0.50 mg mL^{-1} PDDA solution for 5.0 min. (For interpretation of the references to colour in this figure legend, the reader is referred to the web version of this article.)

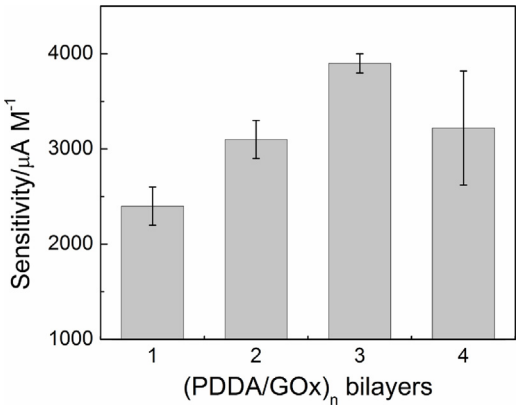

Fig. 4. Sensitivity, obtained from amperometric recordings after successive additions of 5.0×10^{-4} M glucose, as a function of the number of PDDA/GOx bilayers. Working potential: 0.700 V. Supporting electrolyte: 0.050 M phosphate buffer solution pH 7.40. PDDA adsorption conditions: 0.50 mg mL^{-1} PDDA solution for 5.0 min. GOx adsorption conditions: 1.00 mg mL^{-1} GOx solution for 15.0 min.

sensitivity increases with the number of bilayers up to the third one to remain almost constant thereafter.

To obtain additional information from other perspectives that allow a critical analysis of the effect of (PDDA/GOx) bilayers on the performance of the biosensor, the supramolecular architecture was interrogated with different techniques, i.e., EIS, SPR and cyclic voltammetry.

EIS experiments were performed using quinone/hydroquinone (Q/H_2Q) and $[Fe(CN)_6]^{3-/4-}$ as redox markers to evaluate the blockage of the surface and the reversion of the charges during the construction of the multilayers system.

Fig. 5 illustrates the changes in the charge transfer resistances (R_{ct}) for Q/H_2Q at GCE/bCNT-dsDNA after the alternate self-assembling of PDDA and GOx layers. This redox couple is sensitive to the surface blockage as it adsorbs at sp^2 carbon for the electron transfer [24]. The corresponding Nyquist plots and the equivalent circuit (a single time constant-Randles circuit) are shown in Fig. S2 and Scheme S1, respectively (displayed in the Supplementary Information). The R_{ct} increases as a consequence of the blockage of the surface, producing a sluggishness in the charge transfer. A rapid increase of R_{ct} is observed up to the second bilayer, to remain almost constant after the third one, indicating that after the third bilayer there is no appreciable increment in the thickness due to a poor accumulation either of PDDA or GOx.

Considering that the electrostatic interaction between polyelectrolytes is the main driving force when constructing supramolecular architectures based on LbL assembling of polyelectrolytes [25], we performed EIS experiments using the highly-charged redox couple $[Fe(CN)_6]^{3-/4-}$ to evaluate the efficiency of the charge reversion during the multilayers formation. The impedance spectra obtained during the construction of the multistructure using 2.0×10^{-3} M $[Fe(CN)_6]^{3-/4-}$ are depicted in Fig. S3. The fitting of the spectra obtained for the structures ended in PDDA was performed with a single time constant-Randles equivalent circuit. It is important to mention that, although PDDA is usually adsorbed forming loops [26], our results reveal that its coverage is somewhat regular.

The architectures ended in GOx were fitted with a double time constant equivalent circuit (Scheme S2, showed in the Supplementary Information). The theoretical model used in this case was the capillary membrane model [27,28], which has been proposed to study the charge transport through polyelectrolyte multilayers, accounting for the possible defects present in the supramolecular architectures. This model considers that the electrode coverage is not complete in the different stages during the construction of the multilayers delimiting areas more accessible to the electroactive species. In our case, the Nyquist plots corresponding to the architectures ended in GOx are broad and present wide semicircles that are mainly due to the combination of two time constants, indicating the existence of different zones with two different heterogeneous rate constants for $[Fe(CN)_6]^{3-/4-}$ charge transfer [29]. These results suggest that GOx does not fully cover the PDDA layer, with the consequent existence of regions with different coverage of GOx and incomplete charge reversion of PDDA, effect that is more evident after the third layer of GOx. Similar behavior has been reported for other enzyme-polymer LbL assemblies [30] and is associated to the different morphologies of the linear PDDA polymer and the globular GOx protein.

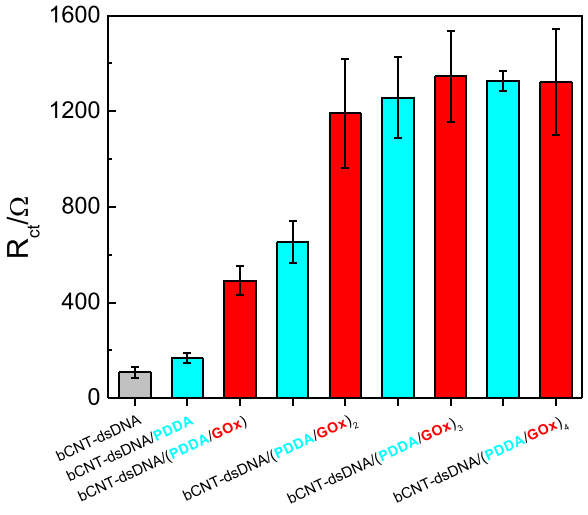

Fig. 5. Dependence of the number of (PDDA/GOx) bilayers with the charge transfer resistance (R_{ct}) obtained from the impedimetric response of quinone/hydroquinone. Amplitude: 10 mV; Frequency range: between 10^5 and 10^{-1} Hz; Working potential: formal potential of a 2.0×10^{-3} M H_2Q/Q solution (~0.050 V). The impedance spectra and equivalent circuits used to fit the experimental data are shown in Supplementary Information, section 2. PDDA and GOx assembling conditions as in Fig. 4.

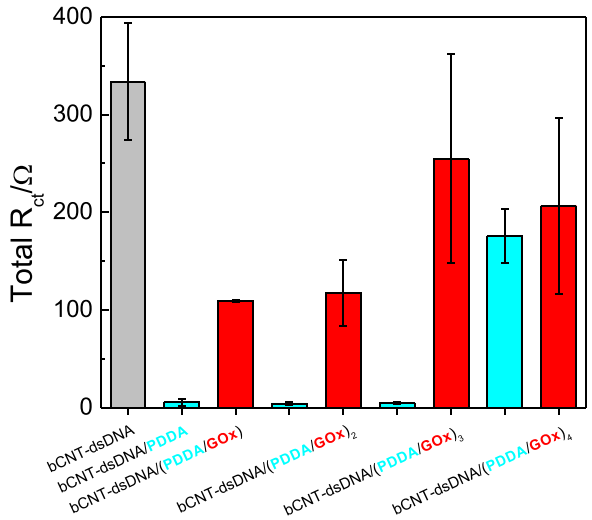

Fig. 6. Dependence of the number of (PDDA/GOx) bilayers with the total R_{ct} obtained from the impedimetric response of $[Fe(CN)_6]^{3-/4-}$. Amplitude: 10 mV; Frequency range: between 10^5 and 10^{-1} Hz; Working potential: formal potential of a 2.0×10^{-3} M $[Fe(CN)_6]^{3-/4-}$ solution (0.210 V). The impedance spectra and equivalent circuits used to fit the experimental data are shown in Supplementary Information, section 2. PDDA and GOx assembling conditions as in Fig. 4.

Fig. 6 shows the variation of the total R_{ct} obtained from the $[Fe(CN)_6]^{3-/4-}$ impedance spectra with the alternate assembling of PDDA and GOx during the construction of the supramolecular architecture. Starting with GCE/bCNT-dsDNA, the total R_{ct} largely decreases after the assembling of PDDA due to the charge reversion and favorable interaction with the highly charged redox marker. The assembling of GOx produces the opposite effect on R_{ct} as a consequence of the repulsion between the redox couple and the negatively charged protein. Thus, a typical "zig-zag" R_{ct} profile [31,32] is observed after alternate immersion of the modified electrode into PDDA and GOx solutions, due to the consecutive electrostatic attraction and repulsion, indicating that the reversion of charges is occurring during the building of the multilayers. At GCE/bCNT-dsDNA/$(PDDA/GOx)_3$, the R_{ct} and the associated uncertainty drastically increases, and after that, the R_{ct} remains almost constant, indicating a poor reversion of charges, effect attributed to the strong interpenetration of the layers. Therefore, at that point the surface blockage becomes the most important factor for the decrease of the apparent charge transfer rate for $[Fe(CN)_6]^{3-/4-}$.

The construction of the supramolecular architecture was also evaluated by SPR. Fig. 7 displays the variation of the surface plasmon resonance angle ($\Delta\theta_{SPR}$) during the assembly of PDDA and GOx layers at bCNT-dsDNA. The inset shows the corresponding sensorgram. The general behavior is that $\Delta\theta_{SPR}$ increases during the alternate adsorption of PDDA and GOx up to the third PDDA/GOx bilayer; however, some differences were found when considering the first, second and third bilayer. For instance, the assembling of the second layers of PDDA and GOx produces increments in $\Delta\theta_{SPR}$ less pronounced than those obtained for the first layers, indicating that the adsorption of PDDA at bCNT-dsDNA is more efficient than at bCNT-dsDNA/PDDA/GOx, mainly due to the different charge density of the surface and local distribution of the negative charges at the electrode surface. After the third bilayer, the changes in the SPR angle are very small evidencing a poor adsorption of PDDA and GOx, in agreement with previous results.

Fig. 8 displays the effect of the number of bilayers on the surface concentration of bioactive GOx (Γ_{GOx}) calculated from the catalytic current density (j_{cat}) for FcOH obtained from cyclic

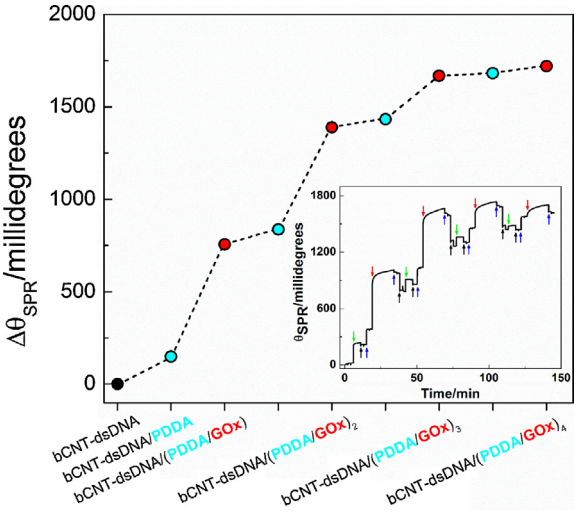

Fig. 7. $\Delta\theta_{SPR}$ values obtained after LbL assembling of PDDA and GOx at GCE/bCNT-dsDNA. Inset: Sensorgram obtained during the LbL assembly of PDDA and GOx at GCE/bCNT-dsDNA. The green and red arrows indicate the injection of PDDA and GOx, respectively; and the black and blue arrows indicate the washing of the surface with water and 0.050 M phosphate buffer pH 7.40, respectively. PDDA and GOx assembling conditions as in Fig. 1. (For interpretation of the references to colour in this figure legend, the reader is referred to the web version of this article.)

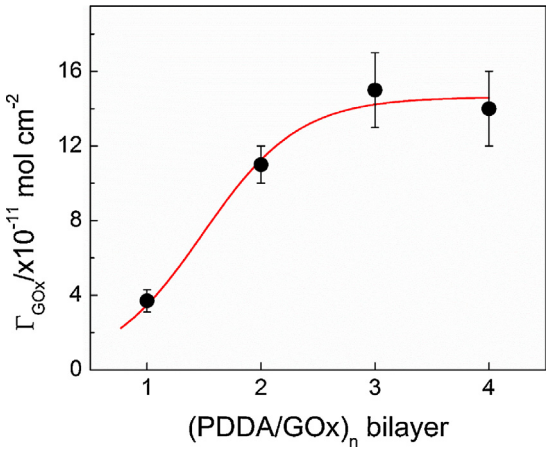

Fig. 8. Surface concentration of bioactive GOx (Γ_{GOx}) as a function of the number of PDDA/GOx bilayers, obtained from voltammetric experiments in 0.30 M glucose using FcOH as redox mediator. Supporting electrolyte: 0.100 M phosphate buffer solution pH 7.40. For further experimental conditions and data fitting, see section 3 in Supplementary Information.

voltammograms performed in the presence of saturation concentrations of glucose (0.30 M) according to the Bourdillon method [33] (for further information, see Supplementary Information). Γ_{GOx} increases with the number of bilayers up to the third one, to remain constant after that, in agreement with the EIS and SPR results previously shown. These results point out that the active site of GOx confined at the electrode surface is accessible to the substrate and that the enzyme retains its biocatalytic activity in the different GCE/bCNT-dsDNA/$(PDDA/GOx)_n$ multistructures.

In fact, the Michaelis-Menten apparent constant (K_M^{app}) for each bilayer obtained from Eadie-Hofstee plots were smaller than the K_M reported for native GOx in solution [34,35]: (1.8 ± 0.7), (0.62 ± 0.08), and (0.21 ± 0.03) mM for the first, second, and third bilayers, respectively (for further information, see section 4 in Supplementary Information). These results suggest that the environment where GOx is immobilized is enzyme-friendly and does not affect significantly the biocatalytic activity of the enzyme.

In summary, the variation of R_{ct}, Γ_{GOx}, $\Delta\theta_{SPR}$ and the sensitivity towards glucose with the number of PDDA/GOx bilayers allow us to get the following conclusions: (i) PDDA and GOx can be successfully assembled at GCE/bCNT-dsDNA to build supramolecular architectures using LbL self-assembly; (ii) the system $(PDDA/GOx)_n$ becomes less stratified as n increases due to interpenetration of the layers; and (iii) GOx incorporated in the supramolecular multistructure retains its biocatalytic activity.

3.3. Analytical performance of the biosensor

The evaluation of the analytical parameters for GCE/bCNT-dsDNA/$(PDDA/GOx)_n$ for n = 1, 2, and 3 indicates that the best analytical performance is obtained with n = 3 (Table 1).

The short-term stability was excellent, even for GCE/bCNT-dsDNA/$(PDDA/GOx)_4$, since the R.S.D. for 10 successive amperometric calibrations for glucose performed at 0.700 V using the

Table 1
Analytical parameters for the quantification of glucose at GCE/bCNT-dsDNA/$(PDDA/GOx)_n$ obtained from amperometric experiments.

	Sensitivity/mA mM^{-1} cm^{-2}	*LOD/mM*	*Linear range/mM*
$(PDDA/GOx)_1$	86 ± 7	0.10	Up to 2.5
$(PDDA/GOx)_2$	172 ± 9	0.10	Up to 3.0
$(PDDA/GOx)_3$	265 ± 7	0.05	Up to 2.0

Table 2
–Comparison of the analytical parameters obtained for GOx-based biosensors using the LbL strategy.

Sensor layer	*Detection*	*Sensitivity/ $\mu A\, mM^{-1}\, cm^{-2}$*	*Linear range/ mM*	*Comments*	Ref.
Au/Cys/(GOx/ amMWCNT)$_4$	Amperometric E = −0.300 V	7.46	1 to 7	Analyzed interferents: AA, UA, PA.	[36]
ITO/PB/(CHIT/MWCNT/ GOx)$_6$	Amperometric E = 0.000 V	8.017	1 to 7	Analyzed interferents: AA, PA.	[37]
GCE/MWCNT/(PEI/ GOx)$_3$/PEI	CV (3rd generation glucose sensor)	106.57	Up to 0.3	Analyzed interferents: AA, UA. Real sample: recovery assay with human serum.	[38]
Au/PB/(CHIT/GOx)$_6$	Amperometric E = 0.000 V	82.8	0.006 to 1.6	Analyzed interferents: AA, UA, PA.	[39]
Au/(MWCNT-MPTS/ AuNPs)$_5$/GOx	Amperometric E = 0.300 V	19.27	0.02 to 10	Analyzed interferents: AA, UA, PA. Real sample: recovery assay with human serum.	[40]
GE/(CRGO/Pyr-GOx)$_3$	Amperometric E = 0.280 V	–	Up to 30	Analyzed interferents: AA, UA. Real sample: recovery assay with human serum.	[41]
Au/(CHIT-NGr-GOx)/ PSS/(CHIT-NGr-GOx)	Amperometric E = −0.200 V	10.5 ± 0.9	0.2 to 1.8	Analyzed interferents: AA, UA, dopamine, citric acid, oxalic acid, fructose, catechol.	[42]
Au/Cys/(Fc-C_6-LPEI/ GOx)$_{16}$/Fc-C_6-LPEI	CV (2nd generation glucose sensor)	15.9	–	–	[43]
Pt/GO/PANHS/GOx	Amperometric E = 0.600 V	40.5 ± 0.4	0.004 to 4.4	–	[44]
GCE/IL-CRGO/S-Gr/GOx/ Naf	Amperometric E = −0.200 V	1.07 ± 0.09	0.01 to 0.5	Analyzed interferents: AA, UA, dopamine. Real sample: in-vivo measurement of glucose in rat striatum using a micro-dialysis system.	[45]
Pt/(PDDA-SWCNT/ GOx)$_7$	Amperometric E = 0.600 V	63.84	0.05 to 12	Analyzed interferents: AA, UA, PA.	[46]
Au/Cys/(GOx/CHIT)$_2$	Amperometric E = 0.300 V	8.91	1.5 to 10.5	–	[47]
GCE/(MWCNT-Polyhys/ GOx)$_5$/Naf	Amperometric E = 0.700 V	27.4 ± 0.4	0.25 to 5	Analyzed interferents: AA, UA, lactose, maltose, galactose. Real sample: milk	[15]
GCE/bCNT-dsDNA/ (PDDA/GOx)$_3$	Amperometric E = 0.700 V	265 ± 7	Up to 2.5	Analyzed interferents: fructose, maltose, galactose, manose. Real sample: beverage, fruit juice and nasal spray.	This work

Symbols: Cys, cysteamine; amMWCNT, aminated MWCNTs; AA, ascorbic acid; UA, uric acid; PA, paracetamol; ITO, idium tin oxide electrode; PB, prussian blue; CHIT, chitosan; PEI: polyethilenimine; MPTS, (3-mercaptopropyl) triethoxysilane; NPs, nanoparticles; GE, graphite electrode; CRGO, chemically-reduced graphene oxide; Pyr, 1-pyrenebuttyric acid; NGr, nitrogen-doped graphene; PSS, polystyrene sulfonate; Fc-C_6-LPEI, linear PEI modified with a ferrocenium group; GO, graphene oxide; PANHS, 1-pyrenebutyric acid-N-hydroxysuccinimide; IL, ionic liquid; S-Gr, sulfonic acid-functionalized graphene; Polyhys, polyhystidine.

same surface (implying more than 180 min of continuous use) was 4.4%.

The interference of other carbohydrates was evaluated from amperometric experiments at GCE/bCNT-dsDNA/(PDDA/GOx)$_3$ at 0.700 V after the addition of 5.0×10^{-3} M Fru, Mal, Gal, and Man, followed by the addition of 5.0×10^{-3} M glucose (the amperometric recordings are depicted in section 5 in the Supplementary Information). No interference was found for Fru, Gal and Mal. In the case of Man (which is a dimer of glucose), there was a small interference (7.2 ± 0.4) % still acceptable from the analytical point of view. Table 2 summarizes the analytical parameters of other LbL-based glucose biosensors. Compared to them, our biosensor, GCE/bCNT-dsDNA/(PDDA/GOx)$_3$, presents a wider linear range and possesses an excellent sensitivity, which is better than those reported by the other strategies.

The GCE/bCNT-dsDNA/(PDDA/GOx) was used to obtain the glucose content in the beverage *"Pepsi-cola"* and the natural orange juice *"Baggio"*. The concentration obtained were (40 ± 4) and (0.6 ± 0.1) x10^2 mg mL^{-1}, respectively, demonstrating an excellent correlation with the values reported by the manufacturer, 39 mg mL^{-1} (Relative Error = 2.5%) and 66.25 mg mL^{-1} (Relative Error = 9.4%) respectively. The glucose content in the nasal spray *"Allennys"*, which contains glucose as an excipient, was also evaluated. The concentrations obtained with GCE/bCNT-dsDNA/(PDDA/GOx)$_n$ with n = 1, 2 and 3 showed an excellent agreement with the value reported in the product (2.75 mg of glucose per dose): (2.6 ± 0.2), (2.9 ± 0.1) and (2.9 ± 0.3) mg of glucose per dose. The excellent correlation demonstrates that GCE/bCNT-dsDNA/(PDDA/GOx)$_n$ is a successful analytical tool for the quantification of glucose. Also, the fine tuning of the sensitivity with the number of bilayers allows reducing the amount of sample used for the determination.

The combination of the excellent dispersing properties of dsDNA, the robustness of the bCNT-dsDNA layer at GCE, the electrocatalytic properties of bCNTs, the negative charge of dsDNA and the biocatalytic specificity of GOx confined at the electrode surface, have allowed us to build up a sensitive, selective, robust, reproducible and stable glucose amperometric biosensor that could be a valuable tool for routine analysis of glucose and quality control in dairy, food and pharmaceutical industries.

4. Conclusions

The results presented here demonstrate the usefulness of bCNT-dsDNA as platform to build biosensing supramolecular architectures. In this particular case, the confluence of the versatility of LbL self-assembling of multilayers, the biocatalytic activity of GOx, the catalytic activity of bCNTs towards the oxidation of the enzymatically generated hydrogen peroxide, and the robustness of CNTs non-covalently functionalized with dsDNA, have allowed the construction of GCE/bCNTs-dsDNA/(PDDA/GOx)$_n$ supramolecular architectures for the sensitive and selective detection of glucose.

The new platform represents an interesting alternative for the development of different types of CNT-based biosensors just varying the bio-recognition element without the need of CNTs pretreatments to generate different functional groups or covalent attachment of bioactive groups.

Acknowledgements

The authors thank CONICET, ANPCyT, SECyT-UNC, MINCyT-Córdoba for the financial support. E.N.P. thanks CONICET for the doctoral fellowship.

Appendix A. Supplementary data

Supplementary data associated with this article can be found, in the online version, at http://dx.doi.org/10.1016/j.electacta.2015.09.028.

References

[1] C.I.L. Justino, A.C. Freitas, R. Pereira, A.C. Duarte, T.A.P. Rocha Santos, Recent developments in recognition elements for chemical sensors and biosensors, TrAC Trends Anal. Chem. 68 (2015) 2–17.
[2] L. Cui, J. Wu, H. Ju, Electrochemical sensing of heavy metal ions with inorganic, organic and bio-materials, Biosens. Bioelectron. 63 (2015) 276–286.
[3] C. Zhu, G. Yang, H. Li, D. Du, Y. Lin, Electrochemical Sensors and Biosensors Based on Nanomaterials and Nanostructures, Anal. Chem. 87 (2015) 230–249.
[4] A. Miodek, G. Castillo, T. Hianik, H. Korri-Youssoufi, Electrochemical aptasensor of human cellular prion based on multiwalled carbon nanotubes modified with dendrimers: A platform for connecting redox markers and aptamers, Anal. Chem. 85 (2013) 7704–7712.
[5] N. Yang, X. Chen, T. Ren, P. Zhang, D. Yang, Carbon nanotube based biosensors, Sensors Actuators B Chem. 207 (2015) 690–715.
[6] J.J. Richardson, M. Bjornmalm, F. Caruso, Technology-driven layer-by-layer assembly of nanofilms, Science 348 (2015) aaa2491.
[7] R.R. Costa, J.F. Mano, Polyelectrolyte multilayered assemblies in biomedical technologies, Chem. Soc. Rev. 43 (2014) 3453–3479.
[8] O.N. Oliveira, R.M. Iost, J.R. Siqueira, F.N. Crespilho, L. Caseli, Nanomaterials for Diagnosis: Challenges and Applications in Smart Devices Based on Molecular Recognition, ACS Appl. Mater. Interfaces (2014) .
[9] W. Yang, D. Trau, R. Renneberg, N.T. Yu, F. Caruso, Layer-by-Layer Construction of Novel Biofunctional Fluorescent Microparticles for Immunoassay Applications, J. Colloid Interface Sci. 234 (2001) 356–362.
[10] W.H. Lin, W.L. Sun, J. Yang, Z.Q. Shen, Preparation and Magnetic Properties of Multilayer Films Based on Self-Assembly, J. Phys. Chem. C 112 (2008) 18217–18223.
[11] F.N. Crespilho, V. Zucolotto, O.N. Oliveira, F.C. Nart, Electrochemistry of layer-by-layer films: A review, Int. J. Electrochem. Sci. 1 (2006) 194–214.
[12] J. Hong, J.Y. Han, H. Yoon, P. Joo, T. Lee, E. Seo, et al., Carbon-based layer-by-layer nanostructures: from films to hollow capsules, Nanoscale 3 (2011) 4515.
[13] Y. Zhang, M.a. Arugula, J.S. Kirsch, X. Yang, E. Olsen, A.L. Simonian, Layer-by-Layer Assembled Carbon Nanotube-Acetylcholinesterase/Biopolymer Renewable Interfaces: SPR and Electrochemical Characterization, Langmuir 31 (2015) 1462–1468.
[14] D. Lee, T. Cui, Layer-by-layer self-assembly of single-walled carbon nanotubes with amine-functionalized weak polyelectrolytes for electrochemically tunable pH sensitivity, Langmuir 27 (2011) 3348–3354.
[15] P.R. Dalmasso, M.L. Pedano, G.A. Rivas, Supramolecular architecture based on the self-assembling of multiwall carbon nanotubes dispersed in polyhistidine and glucose oxidase: Characterization and analytical applications for glucose biosensing, Biosens. Bioelectron. 39 (2013) 76–81.
[16] M. Ma, Z. Miao, D. Zhang, X. Du, Y. Zhang, C. Zhang, et al., Highly-ordered perpendicularly immobilized FWCNTs on the thionine monolayer-modified electrode for hydrogen peroxide and glucose sensors, Biosens. Bioelectron. 64 (2015) 477–484.
[17] Y. Zhang, M.a. Arugula, M. Wales, J. Wild, A.L. Simonian, A novel layer-by-layer assembled multi-enzyme/CNT biosensor for discriminative detection between organophosphorus and non-organophosphrus pesticides, Biosens. Bioelectron. 67 (2015) 287–295.
[18] Q. Cao, J.A. Rogers, Ultrathin films of single-walled carbon nanotubes for electronics and sensors: A review of fundamental and applied aspects, Adv. Mater. 21 (2009) 29–53.
[19] Y.T. Park, J.C. Grunlan, Carbon Nanotube-Based Multilayers, Multilayer Thin Film, Wiley-VCH Verlag GmbH & Co. KGaA, 2012, pp. 595–612.
[20] H. Gao, H. Duan, 2D and 3D graphene materials: Preparation and bioelectrochemical applications, Biosens. Bioelectron. 65 (2015) 404–419.
[21] J. Borges, J.F. Mano, Molecular Interactions Driving the Layer-by-Layer Assembly of Multilayers, Chem. Rev. 114 (2014) 8883–8942.
[22] E.N. Primo, P. Cañete-Rosales, S. Bollo, M.D. Rubianes, G.a. Rivas, Dispersion of bamboo type multi-wall carbon nanotubes in calf-thymus double stranded DNA, Colloid. Surface. B 108 (2013) 329–336.
[23] E.N. Primo, M.B. Oviedo, C.G. Sánchez, M.D. Rubianes, G.a. Rivas, Bioelectrochemical sensing of promethazine with bamboo-type multiwalled carbon nanotubes dispersed in calf-thymus double stranded DNA, Bioelectrochemistry 99 (2014) 8–16.
[24] R.L. McCreery, Advanced Carbon Electrode Materials for Molecular Electrochemistry, Chem. Rev. 108 (2008) 2646–2687.
[25] R.M. Iost, F.N. Crespilho, Layer-by-layer self-assembly and electrochemistry: Applications in biosensing and bioelectronics, Biosens. Bioelectron. 31 (2012) 1–10.
[26] E.S. Forzani, M. López Teijelo, F. Nart, E.J. Calvo, V.M. Solís, Effect of the polycation nature on the structure of layer-by-layer electrostatically self-assembled multilayers of polyphenol oxidase, Biomacromolecules 4 (2003) 869–879.
[27] S.V.P. Barreira, V. Garcia-Morales, C.M. Pereira, J.A. Manzanares, F. Silva, Electrochemical Impedance Spectroscopy of Polyelectrolyte Multilayer Modified Electrodes, J. Phys. Chem. B 108 (2004) 17973–17982.
[28] C. Fernández-Sánchez, C.J. McNeil, K. Rawson, Electrochemical impedance spectroscopy studies of polymer degradation: application to biosensor development, Trends Anal. Chem. 24 (2005) 37–48.
[29] M. Chirea, V. Garcıa-Morales, J.A. Manzanares, C. Pereira, R. Gulaboski, F. Silva, Electrochemical Characterization of Polyelectrolyte/Gold Nanoparticle Multilayers Self-Assembled on Gold Electrodes, J. Phys. Chem. B 109 (2005) 21808–21817.
[30] E. Vázquez, A.E. Aguilar, I. Moggio, E. Arias, J. Romero, H. Barrientos, et al., Immobilization of the enzyme β-lactamase by self-assembly on thin films of a poly(phenylene-ethynylene) sequenced with flexible segments containing sulfur atoms, Mater. Sci. Eng. C 27 (2007) 787–793.
[31] E.J. Calvo, V. Flexer, M. Tagliazucchi, P. Scodeller, Effects of the nature and charge of the topmost layer in layer by layer self assembled amperometric enzyme electrodes, Phys. Chem. Chem. Phys. 12 (2010) 10033–10039.
[32] J.C. Antunes, C.L. Pereira, M. Molinos, F. Ferreira-da-Silva, M. Dessi, A. Gloria, et al., Layer-by-Layer Self-Assembly of Chitosan and Poly(gamma-glutamic acid) into Polyelectrolyte Complexes, Biomacromolecules 12 (2011) 4183–4195.
[33] C. Bourdillon, C. Demaille, J. Gueris, J. Moiroux, J.-M. Savéant, A Fully Active Monolayer Enzyme Electrode Derivatized by Antigen-Antibody Attachment, J. Am. Chem. Soc. 115 (1993) 12264–12269.
[34] G. Palestino, R. Legros, V. Agarwal, E. Pérez, C. Gergely, Functionalization of nanostructured porous silicon microcavities for glucose oxidase detection, Sensors Actuators, B Chem. 135 (2008) 27–34.
[35] H.-Z. Zhao, J.-J. Sun, J. Song, Q.-Z. Yang, Direct electron transfer and conformational change of glucose oxidase on carbon nanotube-based electrodes, Carbon 48 (2010) 1508–1514.
[36] Y. Sun, H. Wang, C. Sun, Amperometric glucose biosensor based on layer-by-layer covalent attachment of AMWNTs and IO_4–oxidized GOx, Biosens. Bioelectron. 24 (2008) 22–28.
[37] Y. Zou, C. Xiang, L. Sun, F. Xu, Amperometric glucose biosensor prepared with biocompatible material and carbon nanotube by layer-by-layer self-assembly technique, Electrochim. Acta 53 (2008) 4089–4095.
[38] C. Deng, J. Chen, Z. Nie, S. Si, A sensitive and stable biosensor based on the direct electrochemistry of glucose oxidase assembled layer-by-layer at the multiwall carbon nanotube-modified electrode, Biosens. Bioelectron. 26 (2010) 213–219.
[39] B. Yin, R. Yuan, Y. Chai, S. Chen, S. Cao, Y. Xu, et al., Amperometric glucose biosensors based on layer-by-layer assembly of chitosan and glucose oxidase on the Prussian blue-modified gold electrode, Biotechnol. Lett. 30 (2008) 317–322.
[40] P. Si, P. Kannan, L. Guo, H. Son, D.-H. Kim, Highly stable and sensitive glucose biosensor based on covalently assembled high density Au nanostructures, Biosens. Bioelectron. 26 (2011) 3845–3851.
[41] J. Liu, N. Kong, A. Li, X. Luo, L. Cui, R. Wang, et al., Graphene bridged enzyme electrodes for glucose biosensing application, Analyst 138 (2013) 2567–2575.
[42] M.M. Barsan, M. David, M. Florescu, L. Tugulea, C.M.A. Brett, A new self-assembled layer-by-layer glucose biosensor based on chitosan biopolymer entrapped enzyme with nitrogen doped graphene, Bioelectrochemistry 99 (2014) 46–52.
[43] J.L. Deluca, D.P. Hickey, D.A. Bamper, D.T. Glatzhofer, M.B. Johnson, D.W. Schmidtke, Layer-by-Layer Assembly of Ferrocene-Modified Linear Polyethylenimine Redox Polymer Films, ChemPhysChem 14 (2013) 2149–2158.
[44] J. Tian, P.-X. Yuan, D. Shan, S.-N. Ding, G.-Y. Zhang, X.-J. Zhang, Biosensing platform based on graphene oxide via self-assembly induced by synergic interactions, Anal. Biochem. 460 (2014) 16–21.
[45] H. Gu, Y. Yu, X. Liu, B. Ni, T. Zhou, G. Shi, Layer-by-layer self-assembly of functionalized graphene nanoplates for glucose sensing in vivo integrated with on-line microdialysis system, Biosens. Bioelectron. 32 (2012) 118–126.
[46] Y. Wang, X. Wang, B. Wu, Z. Zhao, F. Yin, S. Li, et al., Dispersion of single-walled carbon nanotubes in poly (diallyldimethylammonium chloride) for preparation of a glucose biosensor, Sensors Actuators B Chem. 130 (2008) 809–815.
[47] Y. Zhang, Y. Li, W. Wu, Y. Jiang, B. Hu, Chitosan coated on the layers' glucose oxidase immobilized on cysteamine/Au electrode for use as glucose biosensor, Biosens. Bioelectron. 60 (2014) 271–276.